

# EFFICIENT USE OF CEREBRAL CORTICAL THICKNESS TO CORRECT BRAIN MR SEGMENTATION

*Thanh-Mai Diep, Pierrick Bourgeat, Sebastien Ourselin*

BioMedia Lab, Autonomous Systems Laboratory, CSIRO ICT Centre, Brisbane, Australia

## ABSTRACT

Efficient, automatic and robust tools for measurement of cerebral cortical thickness would aid diagnosis and longitudinal studies of neurodegenerative disorders. In this work, we segment a 3D magnetic resonance image of the brain using an Expectation-Maximization approach. The definition of thickness used is based on the solution of Laplace’s equation in the cortex. Unlike other works, finite difference equations for calculation of cortical thickness are generalized for anisotropic images in order to avoid resampling the input images. We also developed a method which combines information from the thickness estimation with the segmentation probability maps, in order to detect missegmented sulci and correct the segmentation accordingly.

**Index Terms**—Cortical thickness estimation, Sulci segmentation

## 1. INTRODUCTION

The cerebral cortex is a sheet of gray matter located on the outer surface of the brain. The gray matter (GM)/white matter (WM) interface is the inner boundary of the cortex, while the gray matter/cerebrospinal fluid (CSF) interface is the outer boundary. Measurement of cortical thickness from 3D magnetic resonance (MR) images can aid diagnosis and longitudinal studies of a wide variety of neurodegenerative and psychiatric disorders, such as Alzheimer’s disease, schizophrenia and epilepsy. Manual measurements are labor intensive, inaccurate and irreproducible.

The segmentation of the cortex is complicated by the presence of noise and a bias field (intensity inhomogeneities). Measurement of cortical thickness also presents several challenges. The definition of cortical thickness is a source of debate and is difficult to define for the highly convoluted topology of the cortex. Definitions of cortical thickness applied by other works include nearest point [1] and coupled surfaces [2, 3]. Unlike these, the Laplacian definition of thickness proposed by Jones *et al.* [4] exhibits uniqueness and reciprocity.

The finite resolution of MRI results in the partial volume effect, where a voxel in an MR image consists of more than one tissue type. Opposite banks of tight sulci may appear fused as CSF is not detected between the folds of gray mat-

ter. This results in erroneously high thickness estimates for these regions. Two approaches for automatic computation of cortical thickness from MR images are the use of deformable models and voxel-based methods.

Zeng *et al.* [2] use coupled surfaces propagation to simultaneously deform two surfaces to fit the inner and outer boundaries of the cortex. The authors (and other works [3]) use a thickness constraint to ensure that the two surfaces remain within a predefined normal range of each other. This approach allows the detection of deep sulci, but may hinder measurement of abnormal cortical thickness. Deformable models are robust to noise and capable of operating in the continuous spatial domain and therefore achieving subvoxel accuracy. However, their major limitation is high processing times in the order of hours [1, 3], attributed to the prevention of self-intersections.

Voxel-based thickness estimation methods are more computationally efficient. Lohmann *et al.* [5] propose a morphology based method to segment and measure gray matter thickness. GM/CSF partial volume voxels between opposing banks of sulci are identified as having neighboring voxels which are closer to white matter, based on a distance transform. However, this method requires removal of noise and intensity inhomogeneities in a prior step. Srivastava *et al.* [6] account for these artifacts during the segmentation and compute cortical thickness using a geodesic distance transform. Lacking in their approach is the detection of sulci, however.

The voxel-based method of Hutton *et al.* [7] uses the Laplacian definition of thickness and thickness information to identify deep sulci. However, no additional information is used to ensure that sulci are correctly identified. Kim *et al.* [8] include mixed tissue classes, as well as pure tissue classes in their segmentation model. Any voxels containing CSF are added to a binary mask, which is skeletonized and defines the outer boundary. This is followed by deforming polygonal meshes to reconstruct the boundaries of the cortex, with a reported processing time of 20 hours [9].

We measure cortical thickness using the Laplacian thickness definition in a voxel-based approach. While other works [4, 5] resample anisotropic (non-uniform voxel dimensions) MR images to obtain isotropic voxels, we generalize the equations for anisotropic data. Haidar *et al.* [10] also solve Laplace’s equation for anisotropic data, but they calculate the thick-

ness by summing the Euclidean distance between neighboring voxels following the streamlines. The approach of Yezzi and Prince [11], which we employ, does not require explicit construction of the streamlines and is not restricted to one neighbor for computation of thickness. We use information from the thickness estimation algorithm, combined with probability maps from the segmentation, to detect and correct the segmentation of deep sulci.

## 2. METHOD

### 2.1. Segmentation

The input MR image is segmented using the statistical algorithm proposed by Van Leemput *et al.* [12]. The intensity histogram of the MR image is modeled as a mixture of Gaussian distributions. The Expectation-Maximization (EM) algorithm is used to iteratively update the model parameters and tissue classifications in order to maximize the likelihood of the image data. Bias field correction and a Markov random field to compensate for noise are included in the EM framework. The resulting output probability maps (soft classifications) for each class are discretized by assigning each voxel to its most likely tissue type.

The algorithm is automatically initialized by *a priori* probability maps for the spatial location of gray matter, white matter and CSF that are affine registered to the MR image using a block matching technique [13]. These *a priori* probability maps are also used during the EM iterations to give spatial information.

### 2.2. Thickness Estimation

A definition of thickness requires a unique association between two points and some definition of thickness between them. We use Laplace's equation, a second order partial differential equation (PDE), to define thickness in the cortex [4]:

$$\nabla^2 f(x, y, z) = \frac{\partial^2 f}{\partial x^2} + \frac{\partial^2 f}{\partial y^2} + \frac{\partial^2 f}{\partial z^2} = 0 \quad (1)$$

The white matter and CSF voxels adjacent to the boundaries of the gray matter are set to fixed potentials. Laplace's equation is then solved in the gray matter volume. The solution  $f(x, y, z)$  is a scalar field which divides the cortex into a set of equipotential sublayers.

The gradient of the Laplace solution is computed using the central differences method and normalized. Each unit vector is perpendicular to the sublayer on which it sits. Starting from a point **a** on the inner boundary, the unit vector field traces a path to a point **e** on the outer boundary (Fig. 1a). This streamline connects pairs of points on the inner and outer boundaries and its length defines thickness in the cortex. This definition of thickness is 3D, unique and robust when applied to the cortex.

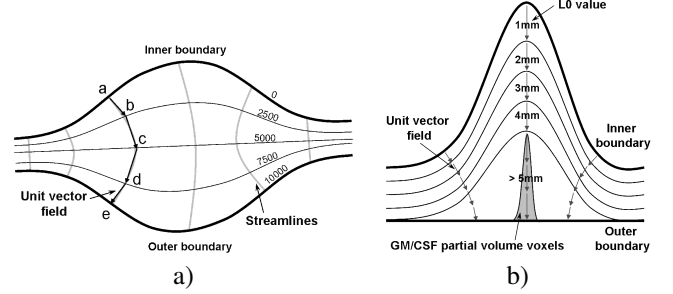


**Fig. 1.** a) The solution of Laplace's equation divides the cortex into equipotential sublayers. b) Sulci detection method uses information from the thickness estimation.

#### 2.2.1. Finite Differences for Anisotropic Images

The method of finite differences approximates PDEs, allowing them to be solved on a discrete grid. Jones *et al.* [4] resample anisotropic MR images using trilinear interpolation to achieve uniform voxel dimensions. Since the segmentation is intensity based, trilinear interpolation would modify the voxel intensities and therefore potentially cause misclassifications. Alternatively, the output probability maps of the segmentation can be resampled. However, interpolation modifies the probability maps and could cause erroneous hard classifications.

To avoid resampling, we solve the Laplace finite difference approximation for anisotropic images iteratively:

$$f_{i+1}(x, y, z) = \frac{1}{2(b^2c^2 + a^2c^2 + a^2b^2)} \left( b^2c^2 [f_i(x+a, y, z) + f_i(x-a, y, z)] + a^2c^2 [f_i(x, y+b, z) + f_i(x, y-b, z)] + a^2b^2 [f_i(x, y, z+c) + f_i(x, y, z-c)] \right) \quad (2)$$

where the spacing between neighbouring voxels in the  $x$ ,  $y$  and  $z$  directions are  $a$ ,  $b$  and  $c$ , respectively;  $f_{i+1}(x, y, z)$  is the potential of the voxel at coordinates  $(x, y, z)$  during the  $(i+1)^{\text{th}}$  iteration.

The length of the streamlines are computed using a pair of first order linear PDEs, proposed by Yezzi and Prince [11]. Let  $L_0(x, y, z)$  be a function that measures the arc length of the streamline from the inner boundary to a point in the gray matter,  $L_1(x, y, z)$  be the arc length of the streamline from the outer boundary to the point, and  $\vec{T}$  be the unit vector that is tangent to the streamline passing through the point. The total length of the streamline through the point is therefore the sum of  $L_0$  and  $L_1$ . The finite difference approximations used to obtain these two functions are also generalized for anisotropic images:

$$L_0(x, y, z) = \frac{1}{bc|T_x|+ac|T_y|+ab|T_z|} \left[ abc + bc|T_x| L_0(x \mp a, y, z) + ac|T_y| L_0(x, y \mp b, z) + ab|T_z| L_0(x, y, z \mp c) \right] \quad (3)$$

$$L_1(x, y, z) = \frac{1}{bc|T_x|+ac|T_y|+ab|T_z|} \left[ abc + bc|T_x| L_1(x \pm a, y, z) + ac|T_y| L_1(x, y \pm b, z) + ab|T_z| L_1(x, y, z \pm c) \right] \quad (4)$$

where

$$x \pm a = \begin{cases} x + a, & T_x > 0 \\ x - a, & T_x < 0 \end{cases} \quad x \mp a = \begin{cases} x - a, & T_x > 0 \\ x + a, & T_x < 0 \end{cases}$$

and similarly for  $y, z, b$  and  $c$ .

The white matter and CSF voxels at the boundaries of the gray matter are initialized to half the negative mean voxel spacing  $-\left(\frac{a+b+c}{6}\right)$ , since distances are measured between the centers of adjacent voxels. Equations (2), (3) and (4) are solved iteratively using the successive overrelaxation (SOR) method. With a good relaxation factor, SOR can require half as many iterations as the Gauss-Seidel method. Based on experiments on real MR images, we chose a relaxation factor of 1.28 for Equation (3) and 1.2 for Equations (3) and (4).

**Table 1.** Synthetic spherical shells 3 mm thick were generated to test the accuracy of the thickness estimation.

Resolution	Axes <sub>x,y</sub>	Axes <sub>z</sub>	Min	Max	Mean
0.5x0.5x0.5	3.00	3.00	2.67	3.08	2.86 ± 0.08
0.5x0.5x1	2.83	3.33	2.47	3.38	2.80 ± 0.16
1x1x1	3.00	3.00	2.37	3.23	2.72 ± 0.17
1x1x1.5	2.83	3.33	2.09	3.37	2.68 ± 0.24

### 2.2.2. Sulci Detection

Sulci detection is performed after one pass of the thickness estimation algorithm. It involves region growing in areas which have thickness values higher than expected for the cortex, and also uses information from the unit vector field and the output probability maps (pmaps) of the segmentation. The sulci detection method concentrates on the outer boundary of the cortex.

The cortex is known to be no thicker than approximately 5 mm [3].  $L_0(x, y, z)$  gives the distance from the inner boundary. Thus regions where  $L_0$  values are greater than 5 mm potentially contain misdetected sulci, composed of GM/CSF partial volume voxels. The gray matter probabilities of these voxels would be lower than pure gray matter voxels.

The sulci detection is illustrated in Fig. 1b and consists of the following steps:

1. Voxels with thickness value greater than 5 mm are placed in a binary mask. The connected components of this mask are labelled. Each component is a local region for finding sulci.

2. The maximum gray matter probability  $p_{max}$  in each thick region is computed. The minimum gray matter probability  $p_{min}$  in the interior of the gray matter is also computed for each thick region. Voxels along the boundaries of the gray matter are excluded from computation of the minimum as they are expected to have low probabilities.

3. If the difference between  $p_{max}$  and  $p_{min}$  are sufficiently high ( $> D$ ), the region potentially contains partial volume voxels. Two thresholds are set,  $t_{min} = p_{min} + A(p_{max} - p_{min})$  and  $t_{max} = p_{min} + B(p_{max} - p_{min})$ .

**Table 2.** Ten isotropic real MR images were subsampled by discarding every second slice. The percentage of voxels ( $\pm$  STDV over 10 images) with thickness values  $>5.5$  mm indicate erroneously thick areas and consider cortical voxels only (i.e. exclude subcortical gray matter and the cerebellum). The mean thickness values ( $\pm$  STDV over 10 images) consider voxels along the inner boundary of the cortex.

Image	Mean thickness (mm)	No. thickness $>5.5$ mm (%)
Isotropic 1x1x1 mm	3.18 ± 0.10	7.26 ± 1.55
Anisotropic 1x1x2 mm	3.41 ± 0.11	10.66 ± 1.58
Resampled MR image (trilinear)	3.63 ± 0.09	11.11 ± 1.90
Resampled pmaps (trilinear)	3.20 ± 0.13	8.50 ± 1.31

4. Gray matter voxels which are in the interior of the gray matter, have  $L_0$  values greater than 5 mm and have less than  $t_{min}$  probability of being gray matter are seeds for the region growing.

5. The region growing process follows the direction of the unit tangent field (towards the outer boundary) to find connected partial volume voxels. Gray matter voxels with probabilities below  $t_{max}$  are added to the seed. The region growing also follows the opposite direction of the unit tangent field to find gray matter voxels with probabilities below  $t_{max}$  and  $L_0$  greater than 5 mm. This is because it is unknown where the seed voxels were situated.

6. After a predefined number of iterations, the region growing stops and the result is skeletonized to obtain one pixel-wide sulci. These voxels are reclassified as CSF.

7. The thickness estimation is re-run within the thick regions.

Experiments on real MR images found that the values  $D = 0.05$ ,  $A = 0.8$ ,  $B = 0.9$  and four region growing iterations give reasonable results.

## 3. RESULTS AND DISCUSSION

We implemented the segmentation and thickness estimation algorithms in C++, as filters for the Insight Segmentation and Registration Toolkit (ITK). On a 2.2 GHz computer, the registration, segmentation and thickness computation (including sulci detection) of a 250x250x180 image take 1.5 minutes, 3 minutes and 1 minute, respectively.

Images of spherical shells with isotropic and anisotropic voxel dimensions were generated to test the accuracy of the thickness estimation (Table 1). For isotropic images, the thickness measurements are accurate along the axes of the sphere. This does not occur for anisotropic images due to the boundary values of Equations (3) and (4) being initialised to negative half of the mean voxel spacing. The higher the difference in the voxel spacings, the higher the error. The thickness is overestimated in one direction, but underestimated in the other direction. Since the cortex is highly convoluted, these are expected to even out.

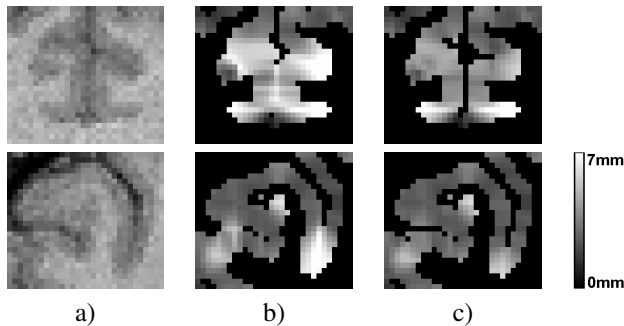


**Fig. 2.** Results of the sulci detection. a) Original MR image, b) Thickness map after first pass of the thickness estimation, and c) Corrected thickness map after second pass.

**Table 3.** The thickness of twenty isotropic real MR images was computed with and without sulci detection. The metrics used are the same as described in Table 2.

Image	Mean thickness (mm)	No. thickness >5.5 mm (%)
No sulci detection	$3.19 \pm 0.12$	$11.77 \pm 1.76$
With sulci detection	$3.15 \pm 0.11$	$6.88 \pm 1.49$

Table 2 compares the thickness measurements of anisotropic images and images which were resampled. Resampling the MR image before segmentation results in greater mean thickness than no resampling because linearly interpolated voxels with intensities intermediate of pure gray and white matter tissues were assigned to the class with the greater variance, which is gray matter. However, resampling of the probability maps resulted in thickness measurements close to the original isotropic images. We conclude that low resolution anisotropic images would benefit from resampling the probability maps, whereas the generalized thickness equations can be applied to high resolution images (i.e.  $0.5 \times 0.5 \times 1$  mm).

Fig. 2 illustrates the correction of the segmentation by the sulci detection. Table 3 shows that sulci detection reduces the number of voxels with erroneously high thickness values. The sulci detection method relies on a reasonable difference between probability values of pure gray matter voxels and partial volume voxels. However, the Markov random field causes the gray matter probabilities to be saturated, thus its strength could be decreased. Alternatively, partial volume estimation could be performed and used instead of probability maps.

#### 4. CONCLUSION

We have presented a fully automated, computationally fast and robust method which segments a 3D MR image and computes the thickness of the cerebral cortex in approximately 5 minutes. The finite difference approximations solved in the thickness estimation are generalized for anisotropic images. Sulci detection decreases the number of erroneously thick areas in the cortex from 12% to 7%.

The accuracy of the thickness estimation depends on the quality of the segmentation. We have successfully combined

information of cortical thickness and tissue probability to improve the segmentation of sulci, which in turn improves the accuracy of the thickness estimation. An avenue for future work could be to include thickness as *a priori* information in the EM segmentation. The sulci detection focuses on the outer boundary of the cortex, but a similar approach could be devised to also detect sulci along the inner boundary. Also in this study, we have confined the search of sulci within regions thicker than 5 mm. However, sulci can also be misdetected in areas where the cortex is extremely thin, and future work will extend this approach to these regions, enforcing a spatial continuity in thickness measurements.

#### 5. REFERENCES

- [1] B. Fischl and A.M. Dale, "Measuring the thickness of the human cerebral cortex from magnetic resonance images," *Proc Natl Acad Sci USA*, vol. 97, pp. 11050–11055, 2000.
- [2] X. Zeng and L.H. Staib *et al*, "Segmentation and measurement of the cortex from 3D MR images using coupled-surfaces propagation," *IEEE TMI*, vol. 18, pp. 927–937, 1999.
- [3] D. MacDonald and N. Kabani *et al*, "Automated 3D extraction of inner and outer surfaces of cerebral cortex from MRI," *NeuroImage*, vol. 12, pp. 340–356, 2000.
- [4] S.E. Jones and B.R. Buckbinder *et al*, "Three-dimensional mapping of cortical thickness using Laplace's equation," *HBM*, vol. 11, pp. 12–32, 2000.
- [5] G. Lohmann and C. Preul *et al*, "Morphology-based cortical thickness estimation," *Inf Process Med Imaging*, vol. 18, pp. 89–100, 2003.
- [6] S. Srivastava and F. Maes *et al*, "An automated 3D algorithm for neo-cortical thickness measurement," in *MICCAI'03*, 2003, vol. 2879, pp. 488–495.
- [7] C. Hutton and E. De Vita *et al*, "Sulcal segmentation for cortical thickness measurements," in *MICCAI'02*, 2002, vol. 2488, pp. 443–450.
- [8] J.S. Kim and V. Singh *et al*, "Automated 3D extraction and evaluation of the inner and outer cortical surfaces using a Laplacian map and partial volume effect classification," *NeuroImage*, vol. 27, pp. 210–221, 2005.
- [9] J.K. Lee and J.M. Lee *et al*, "A novel quantitative cross-validation of different cortical surface reconstruction algorithms using MRI phantom," *NeuroImage*, vol. 31, no. 2, pp. 572–584, 2006.
- [10] H. Haidar and S.V. Egorova *et al*, "New numerical solution of the Laplace equation for tissue thickness measurement in three-dimensional MRI," *J Math Model Algorithms*, vol. 4, pp. 83–97, 2005.
- [11] A.J. Yezzi and J.L. Prince, "An Eulerian PDE approach for computing tissue thickness," *IEEE TMI*, vol. 22, pp. 1332–1339, 2003.
- [12] K. Van Leemput and F. Maes *et al*, "Automated model-based tissue classification of MR images of the brain," *IEEE TMI*, vol. 18, pp. 897–908, 1999.
- [13] S. Ourselin and A. Roche *et al*, "Reconstructing a 3D structure from serial histological sections," *IVC*, vol. 19, pp. 25–31, 2001.